A NEW APPROACH TO ESTIMATE THE IN-SITU THERMAL COEFFICIENT AND DRYING SHRINKAGE FOR JOINTED CONCRETE PAVEMENT

By

Tom Burnham
Research Project Engineer
Minnesota Department of Transportation
Office of Materials and Road Research
1400 Gervais Avenue
Maplewood, MN 55109
Phone: (651) 779-5605
Fax: (651) 779-5616
e-mail: tom.burnham@dot.state.mn.us

and

Amir Koubaa, Post Doctoral Research Associate
University of Minnesota
Department of Civil Engineering
122 Civil Engineering Building
500 Pillsbury Drive S.E.
Minneapolis, Minnesota 55455-0220
Phone: (612) 626-8765
FAX: (612) 626-7750
e-mail: kouba001@tc.umn.edu

Final Manuscript submitted for the
Seventh International Conference on Concrete Pavements

A NEW APPROACH TO ESTIMATE THE IN-SITU THERMAL COEFFICIENT AND DRYING SHRINKAGE FOR JOINTED CONCRETE PAVEMENT

Tom Burnham, Research Project Engineer,
Minnesota Department of Transportation, Maplewood, MN

Amir Koubaa, Post-Doctoral Research Associate,
University of Minnesota, Minneapolis, MN

ABSTRACT

The current development of mechanistic-empirical pavement design methods will necessitate the need for more accurate and realistic material property input values. The Mn/ROAD project was developed and constructed to aid in the determination of those values for pavements in cold climate regions. Utilizing the first 7 years of in-situ strain and temperature data from the Mn/ROAD project, a new approach has been developed for determining the in-situ coefficient of thermal expansion and drying shrinkage of jointed concrete pavements. Correlation analysis between strain and temperature data from embedded vibrating wire strain sensors was performed for six Mn/ROAD concrete pavement test cells. The monthly variation of the in-situ coefficient of thermal expansion was found using the slope between temperature and strain data. The yearly variation in the drying shrinkage was estimated using the intercept from the temperature and strain data. The analysis concluded that the range of in-situ thermal coefficient values is similar to laboratory values reported in the literature for temperatures between –3 and 23°C, and when the concrete moisture content is not high. There was found to be a reduction in the slab strain, equivalent to 8 $\mu\varepsilon/^{o}$C, caused by the effect of slab restraint stresses in the spring and summer seasons. A reduction in the slab restraint effect caused by drying shrinkage as the pavement ages was observed. The joint closure temperature varies seasonally and is significantly affected by the moisture content and temperature of the pavement slab. Utilizing this new approach will enable researchers to better understand the seasonal and age related behavior of the coefficient of expansion and drying shrinkage values for jointed concrete pavements.

INTRODUCTION

Jointed concrete pavements consist of a series of portland cement concrete (PCC) slabs placed over a prepared roadbed. The slabs are exposed to changes in temperature and moisture, as well as to various vehicular traffic loadings. This exposure results in slab deformation, stresses, and strains. PCC pavements are designed to ensure these effects do not result in cracking or faulting of the slabs for a desired amount of service life.

The environmental factors that affect concrete pavement responses the most are the daily temperature changes and seasonal moisture variations. These climatic changes induce two types of deformation in concrete pavement systems:

1) uniform horizontal, caused by changes in the mean slab temperature or moisture content,
2) vertical, induced by temperature and/or moisture content differential across the depth of the slab.

Different provisions are made to take care of the stresses induced by these deformations. The frictional forces of the subbase prevent free movement of the slab, hence inducing longitudinal forces that restrain horizontal movement of the concrete pavement. The magnitude of the subbase restraint depends on the type of subbase and the maximum movement of the joints

(Sargious, 1975). To minimize the effects of frictional stresses in concrete pavements, expansion and/or contraction joints are provided at regular intervals along the length of the pavement.

The most common method available for predicting average horizontal movement of a concrete slab is the general expansion equation [1].

$$\Delta_L = (\Delta_T)\ \alpha_c\ L \qquad [1]$$

where

Δ_T : temperature difference
α_c : coefficient of thermal expansion of concrete
L : panel length

While equation [1] has worked well for general design practice, it does not give a true picture of the joint movement in concrete pavements. The coefficient of thermal expansion (COTE) is not accurately known, as it varies with the type of concrete, subbase material, restraint conditions, and environmental conditions. It has not been proven whether the horizontal movement follows the change in air temperature, pavement surface temperature, or the temperature at some other part of the slab. One study showed that the mid slab movement has a better correlation with the mid-slab temperature change rather than the top or bottom (Jaghoory, 1981). Jaghoory also reported that the stabilized base showed less resistance to both short and long-term movement than the granular base.

Since changing climatic conditions involve variations in precipitation and humidity, both uniform and differential volume changes of the slabs are expected due to varying moisture contents (Bradbury, 1938). Areas of the slabs that are exposed to more moisture (slab bottoms and joint areas) exhibit less moisture shrinkage than the dryer areas of the slab (pavement surface). This produces differential shrinkage between the upper and the lower surfaces of the slab (Janssen, 1994). The amount of drying shrinkage in concrete is a function of mixture proportions, aggregate properties, quality of curing conditions and environmental conditions throughout the lifetime of the pavement.

The changes in the temperature and moisture content in concrete slabs can have a pronounced effect on the apparent coefficient of thermal expansion (COTE). The environmental conditions at the time of curing can have an effect on the overall drying shrinkage of the concrete. Previous attempts to quantify COTE and drying shrinkage behavior in concrete pavement slabs has for the most part been examined through laboratory testing of concrete specimens. Methods to characterize in-situ behavior of these concrete properties would be of great benefit to the next generation of mechanistic-empirical pavement design methods.

OBJECTIVES

The purpose of this paper is to demonstrate a new approach for estimating in-situ values of coefficient of thermal expansion and drying shrinkage for portland cement concrete pavement slabs. Slabs instrumented with vibrating wire strain sensors (VW's) will be selected from six concrete pavement test cells at the Minnesota Road Research project (Mn/ROAD). Seven years of strain and temperature data will be analyzed for 4 VW sensors in each slab considered. From the temperature-strain data, the COTE and drying shrinkage will be estimated based on a linear regression analysis. The effect of slab restraint conditions and seasonal variations on those properties will be described.

THE Mn/ROAD PROJECT

Test section descriptions and selection

Data for this study came from the Mn/ROAD project. Mn/ROAD is an instrumented pavement test facility constructed and maintained by the Minnesota Department of Transportation (Mn/DOT). The facility has over 40 test sections, each containing several types of sensors that can be used to determine the response of a pavement to vehicle loads and environmental effects.

Table 1 summarizes the slab design dimensions and features for the original concrete pavement test cells at Mn/ROAD. Test cells 8 and 9 include an additional concrete inside lane (shoulder), and test cell 40 features thickened-edge panels. Base layer materials consist of special gradations of Mn/DOT class 3, class 4, and class 5 granular materials, as well as permeable asphalt stabilized base (PASB).

The data analyzed for this paper came from Mn/ROAD test cells 5,8,10,11,37, and 38 for the period of September 1993 through October 2000. The test cells were selected based on the quality and quantity of data found in the Mn/ROAD database.

Vibrating wire and thermistor sensors

Vibrating wire strain sensors (VWs) are used to measure "static" (slowly changing) strains resulting from temperature and moisture changes in concrete materials. The vibrating wire sensors at Mn/ROAD are Geokon VCE 4200 Vibrating Wire Strain Gages. Thermistors are built into these sensors so that the temperature in the vicinity of the strain measurement can be recorded. Data is collected from the VW sensors at a rate of one reading approximately every 15 minutes.

The VW sensors were placed in pairs (one gage 2.5 cm from the top of the slab and one 2.5 cm from the bottom of the slab) throughout one slab in each test cell. A typical layout of the vibrating wire sensors at Mn/ROAD is presented in Figure 1. Table 2 summarizes sensor orientation and the slab restraint condition (i.e., doweled or undoweled transverse joints) for test cells containing VW sensors. It should be noted that the transverse joint dowels for several slabs were cut during September 1995 for a Mn/ROAD study on the warp and curl behavior of concrete pavement slabs. The effect of dowel restraint on the slab behavior was not considered in this analysis.

For each test cell considered, four sensors were examined (two sets of stacked sensors), with sequence numbers 8, 11, 15 and 18. As shown in Figure 1, Sensors 8 and 11 are located in the middle of the slab. Sensors 15 and 18 are located near a transverse joint and the shoulder.

COEFFICIENT OF THERMAL EXPANSION

The coefficient of thermal expansion of concrete (α_c in Equation [1] above) is defined as the relative change in length per unit temperature change. The COTE is a function of the type and relative proportions of aggregate and cement paste in the mixture, as well as the moisture content of the concrete. The typical range for the linear coefficient of thermal expansion for cement pastes is from 18 to 20 x 10^{-6} mm/mm/^{o}C. The COTE for concrete coarse aggregates (usually ranging from 6 to 13 x 10^{-6} mm/mm/^{o}C) are generally indicative of laboratory values of COTE for concrete (Metha and Monteiro, 1993).

The thermal coefficient of expansion of concrete consists of the true thermal expansion and the apparent thermal expansion. The true thermal expansion depends on the kinetic molecular movements caused by forces of intermolecular attraction and repulsion. The apparent thermal expansion is caused by "adsorptive mass attraction forces and capillary stresses", also termed "swelling pressure" (Neville, 1987). The apparent thermal expansion occurs in the cement paste region of the concrete. The moisture conditions of concrete typically influence the cement paste portion of the mixture. Temperature increases result in decreases in the capillary tension of the water present and increases in swelling pressure. Swelling pressure does not occur when the concrete is very dry or when it is saturated.

The COTE of concrete has been found to be higher at partially saturated conditions than at extreme moisture conditions (Janssen et al., 1996). Mitchell (1960) noted that the coefficient of thermal expansion is essentially constant over the range from –9.46 to 21.1 ^{o}C in dry concrete whereas moist concrete frequently shows a significant increase in thermal coefficient with increasing temperature.

The coefficient of thermal expansion is of tremendous importance in designing concrete structures. The dimensional instability influences the ability of concrete structures to provide maintenance-free service condition. Expansion and contraction affects concrete pavements in three ways:

1. The presence of temperature and moisture differential between the top and bottom surfaces of the concrete pavement causes curling or warping, respectively (Armaghani, 1987).
2. The expansion and contraction due to uniform temperature change in the entire cross section of the concrete pavement will result in the development of frictional forces between the pavement and the subgrade (Bergstrom, 1950).
3. The presence of compressive stresses in the boundary surface of the pavement caused by rising temperature can lead to blow-ups unless the expansion joints are adequately spaced (Bergstrom, 1950).

DRYING SHRINKAGE

Shrinkage is the decrease of concrete volume with time caused by changes in the moisture content of the concrete and other physicochemical changes. Drying shrinkage occurs after the concrete has already attained its final set and a good portion of the chemical hydration process in the cement gel has been accomplished. Drying shrinkage strains are assumed to be related mainly to the removal of adsorbed water from the hydrated cement paste (Metha and Monteiro, 1993). A portion of the drying shrinkage concrete experiences is recoverable, but typically not to a great extent (Neville, 1987).

The magnitude of drying shrinkage depends on many factors, including the properties of the materials, temperature, relative humidity of the environment, geometry of the concrete element, and the age of the concrete (Neville, 1987). The typical range of drying shrinkage values is 100 to 1,200 x 10^{-6}, with 600 x 10^{-6} being a typical value (Metha and Menteiro, 1993).

Concrete pavements are exposed to both drying and wetting cycles throughout their life. Drying cycles of the pavement cause shrinkage. Wetting cycles cause swelling, which is the increase of

concrete volume with time when the concrete is kept continuously wet (Kosmatka and Panarese, 1992). Shrinkage and swelling are usually expressed as a dimensionless strain (in./in. or mm/mm) under given conditions of relative humidity and temperature.

Since it is directly exposed to the environment, the top surface of a pavement is more susceptible to drying shrinkage than the bottom surface, which is typically exposed to higher moisture levels. This typically creates a shrinkage differential through the slab thickness. Based on the results from field-testing, laboratory testing and computer modeling, Janssen (1987) reported that significant drying in concrete pavement slabs usually occurs at rather shallow depth. This causes shrinkage that is nonlinear throughout the slab thickness and affects concrete pavement in a manner similar to a nonlinear temperature distribution.

NEW APPROACH

Mn/ROAD data

Data from the selected VW sensors was extracted from the Mn/ROAD database for the first 7 years of the project (1993-2000). Following some trial analysis, the data was found best to be broken into monthly periods for each year. This was performed to minimize the variability of the results caused by the effect of seasonal and environmental conditions. Since data was collected every 15 minutes, most data sets within each monthly period consisted of approximately 2,000 to 3,000 data points.

In-situ coefficient of thermal expansion

The in-situ or "apparent" coefficient of thermal expansion (COTE) is estimated from the slope of the best-fit line between measured temperature and strain values as shown in Figure 2. To obtain the actual total strain values, ε_{total} , the VW data from the database had to be corrected using the following equation:

$$\varepsilon_{total} = (R_1 - R_0) + ((T_1 - T_0) * CF_{st}) \quad [2]$$

where:

- ε_{total} : total strain
- R_0 : initial strain value (immediately after paving)
- R_1 : measured strain value at time T_1
- T_0 : initial temperature value (immediately after paving)
- T_1 : measured temperature value at time T_1
- CF_{st}: coefficient of thermal expansion for VW sensor

The second half of equation [2] is used to correct the sensor reading for the difference between the thermal expansion of the steel vibrating wire sensor and the concrete. The in-situ COTE range was compared to laboratory results from Mn/ROAD and values reported in the literature for temperatures between –3 and 23°C.

Drying shrinkage

The in-situ drying shrinkage is estimated using the intercept of the best-fit line of mechanical strain with a selected concrete temperature level. Mechanical strain is of more interest than the total strain when measuring load effects and long term environmental effects in PCC pavements.

The mechanical strain, $\varepsilon_{mechanical}$, is calculated using the following equation:

$$\varepsilon_{mechanical} = (R_1 - R_0) + ((T_1 - T_0) * (CF_{st} - CF_c)) \quad [3]$$

where:

CF_c : coefficient of thermal expansion of concrete (from laboratory tests).

For each month, a temperature level is used to analyze the drying shrinkage effects in the life of the pavement. Different temperature levels for different months are used to minimize the variability of the results from seasonal and environmental effects. The selected temperatures for January to December were –5, -5, 0, 10, 15, 20, 25, 25, 15, 10, 5 and 0 ^oC, respectively. The yearly variation of the net effect of drying shrinkage was analyzed at 23 ^oC after each monthly value was corrected for thermal effects.

Seasonal effects on COTE and drying shrinkage

The period between September 1 and October 30 best estimated the in-situ COTE because the effects of restraint conditions and moisture are minimal and there are no freezing effects. The effect of freezing temperatures was analyzed in the months of December and January because the pavement temperature is mostly below the freezing temperature. The effect of moisture content was analyzed in April and May each year after the thawing period, which usually occurs in March for central Minnesota. In June, the combined effect of moisture content and slightly higher temperature range is analyzed. The effect of high temperature is analyzed in July and August for each year.

INTERPRETATION OF ANALYSIS RESULTS

In situ coefficient of thermal expansion

Figures 2 and 3 show the typical temperature-strain behavior of Mn/ROAD concrete pavement slabs in the longitudinal direction due to temperature and moisture conditions during spring and summer, respectively. Table 3 lists the monthly coefficient of thermal expansion values for test cell 38, sensors 15 and 18. Table 4 presents a statistical summary of the in situ COTE results for sensors 8, 11, 15 and 18 in test cells 5, 8, 10, 11, 37 and 38.

The in-situ COTE values ranged from 6.0 to 13.00 $\mu\varepsilon$ / ^oC. The upper limit of this range indicates that the laboratory COTE obtained from Mn/ROAD cores (approximately 8.0 $\mu\varepsilon/^oC$ shown in Table 1) was lower than the expected value for concrete containing gravel coarse aggregates. This result is expected because the COTE varies with the moisture content and the laboratory values were obtained when the cores were at a fully saturated condition. The lower limit of range in COTE values is caused by slab restraint during transverse joint closure. Figure 4 shows the typical (unrestrained) behavior of concrete in the transverse direction due to temperature and moisture conditions during the summer months.

The upper limit of the in situ COTE is a good estimate of minimal restraint conditions in the concrete. Therefore, the actual COTE of the concrete can be approximately estimated by this upper limit. The difference between the upper limit (13 $\mu\varepsilon/^oC$) and the average in situ COTE (8 $\mu\varepsilon/^oC$) is a reasonable estimate of the base restraint effect, which is equivalent to 5 $\mu\varepsilon/^oC$. No comparison was made between base layer material types for this paper.

During cold periods (below –5 ^{o}C), the in-situ coefficient of thermal expansion was generally higher for most test cells, as shown in Figure 5, especially for the lower portion of the slab (sensors 15 and 18). Possible causes for this could be: 1) greatly reduced transverse joint restraint effects, 2) loss of support caused by temperature gradients, 3) a reduction of base layer friction restraint due to ice formation underneath the pavement slab, or 4) sensor inaccuracies at temperatures below freezing (i.e., the vibrating wire strain sensors are operating outside the manufacturer's recommended functionality range).

The top layer of the concrete slab (sensors 8 and 15) showed a lower thermal expansion coefficient than the bottom of the slab (sensors 11 and 18), which is explained by the effects of moisture conditions and cooling rate. The lower layer of the slab usually has a higher moisture content than the top layer. This causes the concrete to expand more at the bottom layer than the top, resulting in the transverse joints closing sooner near the bottom. The top of the slab is usually subjected to higher temperature and its cooling rate is more rapid than the lower concrete portion.

To more closely examine the daily effects on COTE, the direction of temperature change was analyzed. This analysis showed that for the warming up period (daytime), the COTE was lower than during the cooling period (nighttime) for the same 24-hour period as shown in Figure 6. The top concrete layer has a lower COTE than the bottom concrete layer because the lower concrete portion has a lower cooling rate. The differences of the overall averages are approximately 2.0 $\mu\varepsilon/^{o}$C for cells 10 and 11 (pavement thickness = 24 cm) and 1.5 $\mu\varepsilon/^{o}$C for cells 5, 6, 37 and 38 (pavement thickness' less than 19 cm). Comparison of the nighttime and daytime conditions, within a 24-hour period, showed that the in-situ COTE at night was sometimes higher by as much as 2.5 $\mu\varepsilon/^{o}$C depending on the period of the year and the temperature level. Figure 7 shows that sensor 11, which is located in the middle of the slab and at the bottom of the concrete layer, sometimes demonstrated the opposite trend (i.e., a higher thermal expansion coefficient for warming up periods by as much as 3.5 $\mu\varepsilon/^{o}$C). The reversal of the strain behavior at this location due to heating and cooling might have been caused by the effects of the restraint due to the weight of the slab, base restraint or loss of support caused by a combined effect of moisture and temperature gradients.

Figures 2 and 3 show that when joint closure occurs, the slope of the temperature-strain curve becomes flat for sensors in the longitudinal (parallel to traffic) direction. The reduction in strain due to joint closure is estimated by the difference in slope of the best-fit lines for each portion of the curves. These slope values are a monthly average and vary from cell to cell and sensor to sensor. When the temperature-strain data is analyzed for a single event as shown in Figure 8 (e.g. during a daytime temperature increase), the curve significantly flattens at approximately 5 ^{o}C above the joint closure temperature. For temperatures 5 ^{o}C or higher than the joint closure temperature, a reduction in the strain of approximately 8 $\mu\varepsilon/^{o}$C is observed.

Drying shrinkage

Figure 9 illustrates the variability of the drying shrinkage on a monthly basis as concrete life increases. Figure 10 shows that determining drying shrinkage values should be done for the same period of the year, due to the many factors affecting the mechanical strain level throughout each year. By choosing the same month, the variability due to seasonal variation is minimal.

Drying shrinkage values from the month of October of each year (at a 10 ^{o}C temperature level) were selected for this study.

Table 5 presents the shrinkage values for sensors 8, 11, 15 and 18 in test cells 5, 8, 10, 37 and 38. Sensors 3 and 6 in Cell 5 were added to compare the dry shrinkage values for leave and approach joints. Figures 9 and 10 show that the drying shrinkage effect becomes minimal after 4 to 5 years. Figure 11 illustrates the presence of a differential shrinkage between the top and the bottom of the concrete slab.

The drying shrinkage varied between cells and sensor locations. The top concrete layer exhibited a higher shrinkage than the bottom concrete layer. As shown in Table 6, the drying shrinkage per linear cm for thin pavement is higher (nearly double) than for thick pavements. Figure 12 shows the same trends and differences between top and bottom when the mechanical strain is analyzed for any period of the year. The drying shrinkage is also higher near the joint than in the middle of the slab. The reduction in drying shrinkage in the middle of the slab might have been caused by the effect of fewer wetting and drying cycles, less moisture at this location or higher restraint effects due to subbase material and/or weight of the slab.

Analysis of the joint closure

Joint closure effect, predominantly in the longitudinal (with traffic) direction, is reflected by a bend in the curve on temperature-strain plots. The temperature at which the curve significantly changes slope is deemed the joint closure temperature, T_c. Joint closure temperatures from this analysis are summarized in Tables 7 and 8. Due to differing seasonal moisture conditions in the slab, the data was analyzed for two periods, spring (April and May) and summer (June-September).

Tables 7 and 8 show that the spring joint closure temperature is on average 7 ^{o}C lower than the summer values. Higher temperatures during the summer seasons reduce the available moisture to the slab, which therefore requires more temperature-related expansion before joint closure. Thus, an average effect of 56 με (equivalent to a 7 ^{o}C temperature change) is resulting from the moisture content effect in the spring season, which is equivalent to a joint movement of 0.2, 0.26, 0.34 and 0.41 mm for cells with panel lengths of 3.6, 4.6, 6.1 and 7.3 m; respectively. In the middle of the slab, the locking of horizontal movement for top and bottom of the concrete layers are relatively equal or are within 2 ^{o}C of each other. However, for the edge sensors, the joint closure temperature difference between top and bottom layers is within 5 ^{o}C. The joint closure temperatures for cell 5 are shown in Figures 13 and 14 and illustrate the above trends.

Analysis of cell 10 in March and April 1998 showed that for the spring season, the bottom layer near the transverse joint locks first and the top layers lock at a later time (approximately 2 to 4 hours). The bottom sensors in the middle of the slab and near the joint locked approximately at the same time. Similar analysis for cell 10 in July and August 1998, showed that the top layer of the concrete slab near the transverse joint locks first and the lower layer locks at a later time (approximately 4 hours). The bottom sensors showed that the bottom concrete layer near the joint locked approximately 2 hours prior to the middle of the slab.

Figures 13 and 14 also demonstrate that the joint closure temperature increases with age. This increase is estimated between 2 to 5 ^{o}C for the period of April 1994 to October 2000. The average increase for sensor 15 in Cell 10 was also estimated for July and August in 1995 and 2000 using closure event data. This analysis showed that the joint closure temperatures increase are 2.5 and 1.5 ^{o}C; respectively. This increase is likely related to drying shrinkage of the slab over time and/or wearing of the joint faces.

The above results demonstrate that the joint closure temperature varies with the depth and the location in the slab and the age of the pavement. The transverse joint closure also resulted in restraining the middle of the slab in the longitudinal direction. The longitudinal movement due to the restraint effect differential between the top and bottom near the transverse joint is estimated between 16 to 40 με (caused by a 2 to 5 ^{o}C temperature difference). Therefore, the temperature gradient, temperature level, moisture level, joint closure temperature and its seasonal variations affect the deflected shape of the slab.

CONCLUSIONS

The current development of mechanistic-empirical concrete pavement design methods will soon demand better characterization of material properties for reliable results. The methods outlined in this paper for determining the in-situ coefficient of thermal expansion and drying shrinkage of concrete pavement slabs will be beneficial toward that effort.

Based on an extensive analysis of Mn/ROAD vibrating wire strain sensor data, the following conclusions and recommendations can be drawn:

1. The vibrating wire data was successfully used to estimate the in-situ COTE and drying shrinkage of PCC concrete pavement. This data has quantified several pavement phenomena such as joint closure restraint effect, drying shrinkage, and differential shrinkage between the top and bottom of PCC pavements.
2. The range of in-situ COTE values was found to be similar to laboratory values reported in the literature. The joint closure temperature is used as an upper cut off temperature to obtain the in situ COTE.
3. A reduction in the strain, equivalent to 8 με/^{o}C, is observed and caused by the effect of restraint stresses in the spring and summer seasons. This reduction is caused by the closure of the joint and its effect is maximized when the pavement temperature is approximately 5 ^{o}C higher than the closure temperature.
4. The lower portion of a concrete slab usually has a higher COTE value because of the effect of cooling rate and moisture content.
5. The joint closure temperature varies seasonally and is significantly affected by the moisture content and temperature of the pavement slab. The joint closure temperature varies across the depth of the pavement slab.
6. A differential drying shrinkage was observed between the top and bottom of the concrete slab. The top of the slab exhibited a higher drying shrinkage than the bottom of the slab. The concrete near the transverse joint also exhibited a higher shrinkage than the middle of the slab.
7. Drying shrinkage and/or joint wearing results in an increase in the closure temperature during the first few years of a pavement's life.

8. The vibrating wire strain gages might have a lower temperature functioning range then the one specified by the manufacturer.
9. The effects of aggregate type and paste properties on the COTE and drying shrinkage can be analyzed in the field using vibrating wire strain sensors embedded in the concrete. Similar techniques and analysis might be performed on laboratory specimens.
10. To analyze the deflected shape of the slab for curling and warping analysis, the temperature gradient, temperature level, moisture content and joint closure temperature (and its seasonal variations) should be known.
11. Vibrating wire data can be used to analyze the effect of construction season on the differential shrinkage between the top and bottom of a concrete slab.

DISCLAIMER

The contents and opinions presented in this paper are those of the authors, who are responsible for the facts and the accuracy of the data. The contents do not necessarily reflect the views or opinions of the Minnesota Department of Transportation.

LIST OF REFERENCES

Armaghani, J.M. *Comprehensive Analysis of Concrete Pavement Response to Temperature and Load Effects.* Ph.D. Thesis, University of Florida. Florida, 1987.

Bergstrom, S.G. "Temperature Stresses in Concrete Pavements*." Proceedings of the Swedish Cement and Concrete Research Institute*, No. 14. Sweden, 1950. Pp. 1-37.

Bradbury, R.D. *Reinforced Concrete Pavements*. Wire Reinforcement Institute, Washington, D.C., 1938.

Jaghoory, S. *Effects of Various Design Parameters on the Movement of Jointed Concrete Pavements.* Ph.D. Thesis, University of Cincinnati, OH,1981.

Janssen, D.J. "Early and Long Term Effects of Curling and Warping on Jointed Concrete Pavement." *Technical Proposal*. University of Washington, Seattle, WA, 1994.

Janssen, D.J. "Moisture in Portland Cement Concrete." *Transportation Research Record 1121*. Transportation Research Board, National Research Council, Washington, D.C., 1987.

Janssen, D.J., B.M. Savage, E.E. Holt, M.B. Snyder, M.J. Sheehan. "Early and Long-Term Effects of Curling and Warping on Jointed Concrete Pavements." *Interim Report Part II: Experimental and Gradient Modeling Plan*. FHWA Contract DTFH61-95-C-00021, Seattle, WA, 1996.

Kosmatka, S.H. and W.C. Panarese. *Design and Control of Concrete Mixtures*, 13th Edition. Portland Cement Association. Skokie, Illinois. 1992.

Metha, P.K. and P.J.M. Monteiro. *Concrete: Structure, Properties, and Materials*, Second Edition. Prentice-Hall, Inc., Englewood Cliffs, NJ, 1993.

Mitchel, R.G. "The Problem of Corrosion of Load Transport Devices." *Highway Research Board Bulletin 274*. Highway Research Board, Washington D.C., 1960.

Neville, A.M. *Properties of Concrete*, Third Edition. Longman Scientific and Technical with John Wiley and Sons, Inc., New York, NY, 1987.

Sargious, Michel. *Pavements and Surfacing for Highways and Airports*. John Wiley and Sons, New York, NY, 1975.

Table 1: Mn/ROAD concrete slab design details

Test Cell	Design Life	Construction Date	Slab Thickness (cm)	Slab Length (m)	Panel Widths Inside/Outside Lanes (m)	Subbase Type	Subbase Thickness (cm)	Dowel Diameter (cm)	Edge Drain	Thermal Coefficient $\mu\varepsilon/^{o}C$ (1)
5	5-Year	9/15/1992	19	6.1	4.0/4.3	cl4sp(2) over cl3sp(3)	7.6, 68	2.5	No	8.1×10^{-6}
6	5-Year	9/15/1992	19	4.6	4.0/4.3	cl4sp	12.7	2.5	No	8.1×10^{-6}
7	5-Year	9/16/1992	19	6.1	4.0/4.3	PASB(4) over cl4sp	10, 7.6	2.5	Yes	8.1×10^{-6}
8	5-Year	9/16/1992	19	4.6	4.0/4.0/4.3	PASB over cl4sp	10, 7.6	2.5	Yes	8.4×10^{-6}
9	5-Year	9/16/1992	19	4.6	4.0/4.0/4.3	PASB over cl4sp	10, 7.6	2.5	Yes	9.8×10^{-6}
10	10-Year	6/14/1993	24	6.1	3.7/3.7	PASB over cl4sp	10, 7.6	3.2	Yes	6.7×10^{-6}
11	10-Year	6/14/1993	24	7.3	3.7/3.7	cl5sp(5)	12.7	3.2	No	6.7×10^{-6}
12	10-Year	6/14/1993	24	4.6	3.7/3.7	cl5sp	12.7	3.2	Yes	8.8×10^{-6}
13	10-Year	6/14/1993	24	6.1	3.7/3.7	cl5sp	12.7	3.8	No	8.8×10^{-6}
36	LVR	7/19/1993	15	4.6	3.7/3.7	cl5sp	12.7	2.5	No	8.4×10^{-6}
37	LVR	7/19/1993	15	3.6	3.7/3.7	cl5sp	30.4	n/a	No	8.4×10^{-6}
38	LVR	7/19/1993	15	4.6	3.7/3.7	cl5sp	12.7	2.5	No	8.4×10^{-6}
39	LVR	7/19/1993	15	6.1	3.7/3.7	cl5sp	12.7	2.5	No	8.4×10^{-6}
40	LVR	7/19/1993	19/16/19	4.6	3.7/3.7	cl5sp	12.7	n/a	No	8.4×10^{-6}

(1): Thermal coefficient was determined from laboratory samples

(2): cl4sp: Mn/DOT Class 4 granular base material with special crushing requirement (no crushed/fractured particles)

(3): cl3sp: Mn/DOT Class 3 granular base material with special crushing requirement (no crushed/fractured particles)

(4): PASB: Permeable Asphalt Stabilized Base

(5): cl5sp: Mn/DOT Class 5 granular base material with special crushing requirement (10 - 15% crushed/fractured particles are required)

Table 2: Orientation of vibrating wire sensors and slab restraint condition

Test Cell	Top Gage Orientation	Bottom Gage Orientation	Restraint Condition
5	Longitudinal	Longitudinal	unrestrained[1]
6	Longitudinal	Longitudinal	restrained
8	Longitudinal	Transverse	unrestrained[1]
9	Transverse	Longitudinal	restrained
10	Longitudinal	Longitudinal	restrained
11	Transverse	Transverse	unrestrained[1]
36	Longitudinal	Longitudinal	restrained
37	Transverse	Longitudinal	unrestrained
38	Transverse	Transverse	restrained

(1): Test cell was originally doweled. Dowels were cut in September 1995.

Table 3: In-situ coefficients of thermal expansion for Cell 38, sensors 15 and 18

	38-VW-15			38-VW-18		
Month (March - November)	In-Situ Thermal Expansion Coefficient (με/°C)	Best Fit Line Intercept (με/oC)	Correlation Coefficient, R^2	In-Situ Thermal Expansion Coefficient (με/°C)	Best Fit Line Intercept (με/°C)	Correlation Coefficient, R^2
Apr-94	6.69	-240.58	0.91	8.84	-154.96	0.99
Jun-94	8.71	-287.74	0.95	9.60	-186.55	0.97
Oct-94	8.84	-284.87	0.99	9.79	-206.07	0.97
Apr-95	7.70	-256.28	0.99	8.09	-182.96	0.97
Jun-95	6.54	-226.43	0.86	10.23	-240.66	0.99
Oct-95	7.60	-320.76	0.97	8.73	-204.22	0.98
Apr-96				8.88	-175.11	0.98
Jun-96	8.96	-352.84	0.94	10.11	-215.49	0.99
Oct-96	7.61	-345.68	0.92	9.36	-208.22	0.98
Apr-97				8.84	-171.97	0.98
Jun-97	9.43	-367.36	0.97	10.73	-227.74	0.98
Oct-97	8.11	-338.82	0.98	8.80	-186.68	0.99
Apr-98				9.57	-175.90	0.99
Jun-98	9.25	-346.89	0.99	9.93	-195.88	0.98
Oct-98	8.92	-335.19	0.90	10.12	-196.95	0.97
Apr-99	7.52	-283.79	0.96	9.28	-161.94	0.99
Jun-99	8.97	-337.35	0.97	10.22	-196.95	0.99
Oct-99	9.31	-347.21	0.98	9.16	-165.31	0.97
Apr-00	7.85	-290.50	0.95	9.05	-150.99	0.99
Jun-00	7.69	-312.92	0.90	9.20	-168.74	0.97
Oct-00	10.34	-365.24	0.87	9.56	-168.60	0.98
Maximum	10.34	-226.43	0.99	10.73	-150.99	0.99
Minimum	6.54	-367.36	0.86	8.09	-240.66	0.97
Standard Deviation	1.01	42.85	0.04	0.64	23.80	0.01
Count	18	18	18	21	21	21
Median	8.41	-327.98	0.96	9.36	-186.55	0.98
Average	8.34	-313.36	0.94	9.43	-187.71	0.98

Winter Months (December - February)	In-Situ Thermal Expansion Coefficient (με/°C)	Best Fit Line Intercept (με/°C)	Correlation Coefficient, R^2	In-Situ Thermal Expansion Coefficient (με/°C)	Best Fit Line Intercept (με/°C)	Correlation Coefficient, R^2
Maximum	13.31	-250.26	0.98	15.89	-130.23	0.99
Minimum	7.76	-317.77	0.85	10.69	-169.76	0.87
Standard Deviation	1.40	19.09	0.04	1.36	12.96	0.03
Count	18	18	18	18	18	18
Median	11.45	-284.76	0.95	14.12	-150.62	0.97
Average	11.12	-282.68	0.94	13.93	-150.36	0.95

Table 4: Statistical summary of in-situ coefficients of thermal expansion for various Mn/ROAD test cells

	05VW08			10VW08			37VW08		
Statistics	**In-Situ Thermal Expansion Coefficient ($\mu\varepsilon/^oC$)**	**Best Fit Line Intercept ($\mu\varepsilon/^oC$)**	**Correlation Coefficient, R^2**	**In-Situ Thermal Expansion Coefficient ($\mu\varepsilon/^oC$)**	**Best Fit Line Intercept ($\mu\varepsilon/^oC$)**	**Correlation Coefficient, R^2**	**In-Situ Thermal Expansion Coefficient ($\mu\varepsilon/^oC$)**	**Best Fit Line Intercept ($\mu\varepsilon/^oC$)**	**Correlation Coefficient, R^2**
Maximum	9.50	-207.00	0.96	9.17	-331.05	0.95	11.39	-215.74	0.99
Minimum	6.32	-310.27	0.71	5.90	-516.92	0.28	6.20	-303.94	0.69
Standard Dev	0.69	24.76	0.00	0.71	38.83	0.01	1.26	16.24	0.00
Average	7.66	-273.47	0.89	7.81	-460.46	0.78	8.30	-252.30	0.94

	05VW11			10VW11			37VW11		
Maximum	12.56	-228.17	0.99	11.79	-312.72	0.98	13.56	-242.03	0.98
Minimum	6.84	-392.60	0.51	6.96	-473.87	0.42	6.23	-366.40	0.58
Standard Dev	1.35	35.37	0.00	0.86	28.61	0.00	2.09	36.27	0.00
Average	9.89	-295.77	0.80	9.95	-400.86	0.84	9.84	-289.39	0.87

	05VW15			10VW15			37VW15		
Maximum	10.43	-296.77	1.00	10.95	-411.63	0.99	10.90	-274.87	0.99
Minimum	7.21	-441.02	0.81	7.73	-641.83	0.86	7.00	-459.98	0.88
Standard Dev	0.62	30.39	0.00	0.71	55.99	0.00	0.90	45.23	0.00
Average	9.22	-371.88	0.97	9.40	-540.01	0.96	8.90	-345.59	0.97

	05VW18			10VW18			37VW18		
Maximum	12.70	-185.01	1.00	12.52	-387.77	0.99	12.88	-220.91	0.99
Minimum	4.25	-281.47	0.08	5.29	-593.23	0.21	6.62	-364.90	0.81
Standard Dev	1.57	19.24	0.01	1.07	41.95	0.01	1.67	37.04	0.00
Count	72.00	72.00		59.00	59.00		36.00	36.00	
Median	8.87	-236.26	0.95	9.80	-502.66	0.94	9.49	-262.25	0.97
Average	8.92	-238.61	0.92	9.92	-501.17	0.87	9.73	-271.97	0.95

	08VW08			11VW08			38VW08		
Maximum	10.37	-348.99	0.99	11.39	-215.74	0.99	13.20	-228.78	0.99
Minimum	7.83	-513.35	0.79	6.20	-303.94	0.69	7.47	-379.15	0.47
Standard Dev	0.57	33.83	0.00	1.26	16.24	0.00	1.56	29.25	0.00
Average	9.07	-447.89	0.97	8.30	-252.30	0.94	9.34	-272.95	0.90

	08VW11			11VW11			38VW11		
Maximum	11.53	-306.20	0.98	13.86	-162.27	0.99	17.87	-118.85	0.98
Minimum	7.49	-485.63	0.65	8.17	-300.29	0.05	7.06	-322.31	0.63
Standard Dev	0.98	47.45	0.00	1.42	31.09	0.01	2.38	43.47	0.00
Average	9.88	-399.90	0.93	10.51	-206.08	0.90	10.93	-222.95	0.92

	08VW15			11VW15			38VW15		
Maximum	10.29	-382.99	1.00	11.70	-335.40	1.00	13.31	-226.43	0.99
Minimum	7.88	-506.78	0.70	7.76	-521.12	0.86	6.54	-425.68	0.77
Standard Dev	0.52	32.22	0.00	0.81	46.66	0.00	1.55	42.40	0.00
Average	9.18	-446.41	0.97	9.56	-427.27	0.96	9.28	-313.30	0.94

	08VW18			11VW18			38VW18		
Maximum	11.63	-185.66	0.99	14.87	-112.89	0.98	15.89	-130.23	0.99
Minimum	7.94	-479.96	0.80	8.35	-262.84	0.27	8.09	-270.40	0.74
Standard Dev	0.86	68.94	0.00	1.64	31.84	0.01	2.09	33.83	0.00
Average	9.86	-379.76	0.97	10.71	-174.41	0.89	11.11	-184.90	0.97

Table 5: Estimated drying shrinkage values (in με) for October at 10^{E}C

Age (months)	0	13	25	37	61	73	85	97
05VW03	-35	-203	-187	-234				
05VW06	-30	-108	-151	-186	-156	-156	-148	-162
05VW08	-34	-66	-105	-117	-146	-130	-138	-131
05VW11	-31	-103	-125	-136	-147	-146	-130	-140
05VW15	-35	-169	-191	-204	-232	-229	-225	-231
05VW18	-30	-61	-80	-115	-95	-83	-72	-70
Age (months)	**0**	**25**	**37**	**49**	**61**	**73**	**85**	**97**
08VW08	-66	-188	-219	-247	-238	-234	-239	-238
08VW11	-65	-108	-138	-162	-166	-177		-173
08VW15	-65	-170	-208	-234	-233	-236		-234
08VW18	-67	-121	-150	-159	-155	-169	-156	-165
Age (months)	**0**	**5**	**17**	**29**	**41**	**53**	**65**	**77**
10VW08	-32	-198	-235	-263	-268	-276		
10VW11	-38	-169	-204	-220	-245	-242	-245	-237
10VW15	-30	-222	-271	-314	-330	-333	-373	-377
10VW18	-37	-201	-263	-279	-280	-284		
Age (months)	**0**	**4**	**16**	**28**	**40**	**52**	**64**	**76**
37VW08	-63	-31	-35	-50	-34			
37VW11	-62	-63	-86					
37VW15	-64	-68	-79	-128	-124	-144	-157	-169
37VW18	-62	-36	-50	-75				
Age (months)	**0**	**4**	**16**	**28**	**40**	**52**	**64**	**76**
38VW08	-46	-80	-87	-108				
38VW11	-50	12	-25	-26	-9	-28	-21	-39
38VW15	-48	-77	-132	-156	-141	-127	-134	-149
38VW18	-51	16	9	8	27	28	51	49

Table 6: Estimated drying shrinkage differential between top and bottom of concrete (in με; month = Oct.; T = 10EC; Age = 50 months)

Top Sensor	Bottom Sensor	Top Drying Shrinkage value (me)	Bottom Shrinkage Value (me)	Difference in με = (Top - Bottom)	Difference in με/cm = (Top - Bottom)
05VW03	**05VW06**	-275	-155	-120	-11.8
05VW08	**05VW11**	-150	-145	-5	-0.5
05VW15	**05VW18**	-230	-90	-140	-13.1
08VW08	**08VW11**	-240	-180	-60	-5.6
08VW15	**08VW18**	-235	-160	-75	-7.2
10VW08	**10VW11**	-280	-240	-40	-2.6
10VW15	**10VW18**	-370	-285	-85	-5.7
37VW15	**37VW18**	-170	-80	-90	-10.7
38VW08	**38VW11**	-110	-25	-85	-9.8
38VW15	**38VW18**	-145	45	-190	-22.0

Table 7: Spring season joint closure temperatures for VW sensors mounted longitudinally

	Joint Closure Temperature (°C)									
	05VW08	05VW11	05VW15	05VW18	08VW08	08VW15	10VW08	10VW11	10VW15	10VW18
Age (months)	Top	Bottom	Top	Bottom	Top	Top	Top	Bottom	Top	Bottom
10							17		24	16
11							29	25	30	27
19	17	16	21	13						
20	24	25	27	17						
22							16		20	
23							23	21	26	22
32	21	19								
34							15		22	16
35							25	24	27	19
44				23	28	30				
46							16	15	20	15
47							24	18	23	18
55	13	17		16						
56	20	20	28	22	27	32				
58							25	20	24	19
59							26	22	27	22
67			28	21	27					
68	26	29	30	22	30	38				
70								17	23	17
71								20	27	21
80			28	28	33					
82								18	23	
91	23	20	25	20	25	31		22	28	
92	26	26	30	26	30	34				

Table 8: Summer season joint closure temperatures for VW sensors mounted longitudinally

	Joint Closure Temperature (°C)									
	05VW08	05VW11	05VW15	05VW18	08VW08	08VW15	10VW08	10VW11	10VW15	10VW18
Age (months)	Top	Bottom	Top	Bottom	Top	Top	Top	Bottom	Top	Bottom
12							31	27	30	29
21	26	26	29	22						
24							30	28	30	25
33	28	30	33							
35	30	28	36							
36	30	28		27			29	25	30	23
39							30		32	24
45	30	29	36	31	35	35				
47	32	28	37	31	35	39				
48							29	24	27	24
51							30	24	29	24
57	30	27	32		33	37				
58	30	32	37	32	34	41				
59	26	35			29	41				
60	26	25		25			27	22	29	22
61							29	27	31	28
70	34	30	40	33	37	40				
71	31	31	36	30	37	39				
72								23	28	22
81			32		31					
82	33	34	37		37					
84			34	26				25	29	
93	30	29	35	27	32					
94	36	32	39	32	36	39				

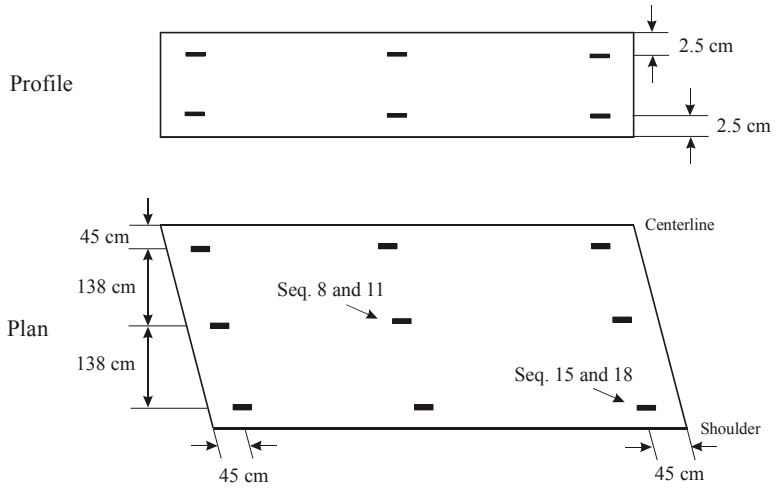

Figure 1: Layout of vibrating wire strain gages at Mn/ROAD

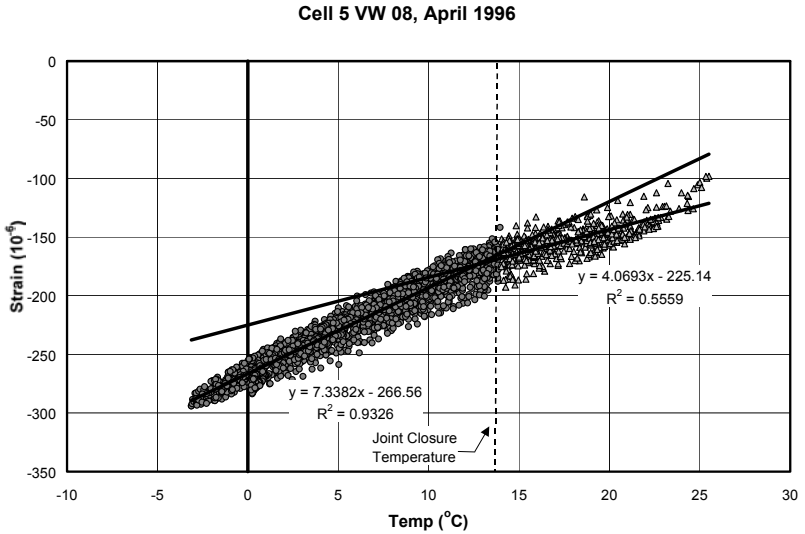

Figure 2: Typical strain versus temperature for longitudinal vibrating wire strain sensor data (Spring)

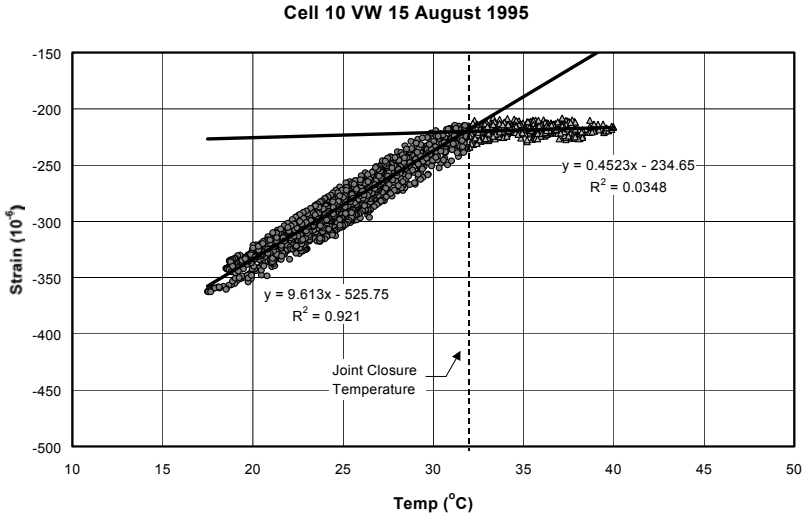

Figure 3: Typical strain versus temperature for longitudinal vibrating wire strain sensor data (Summer)

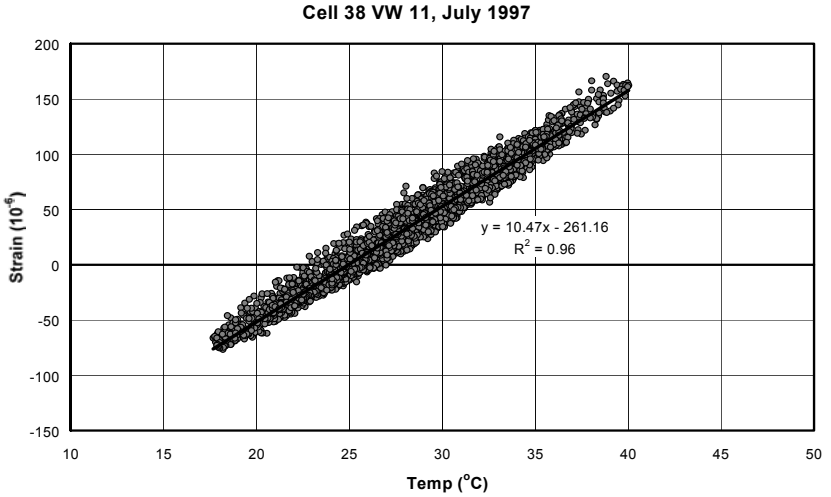

Figure 4: Typical strain versus temperature for transverse vibrating wire strain sensor data (Summer)

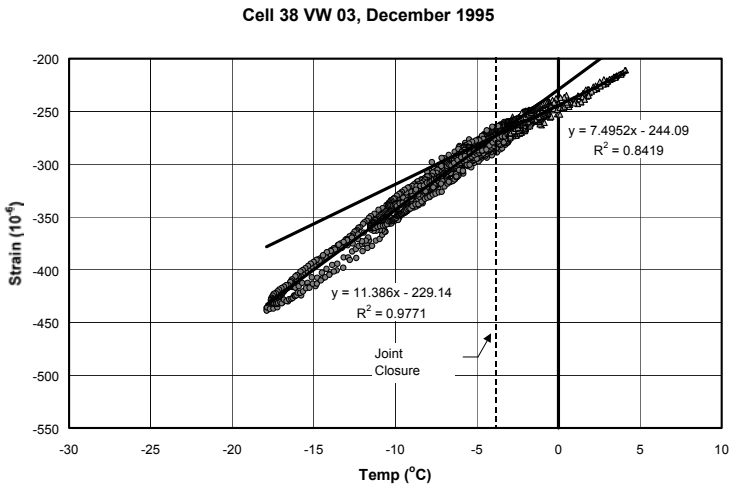

Figure 5: Typical strain versus temperature for longitudinal vibrating wire strain sensor data (Winter)

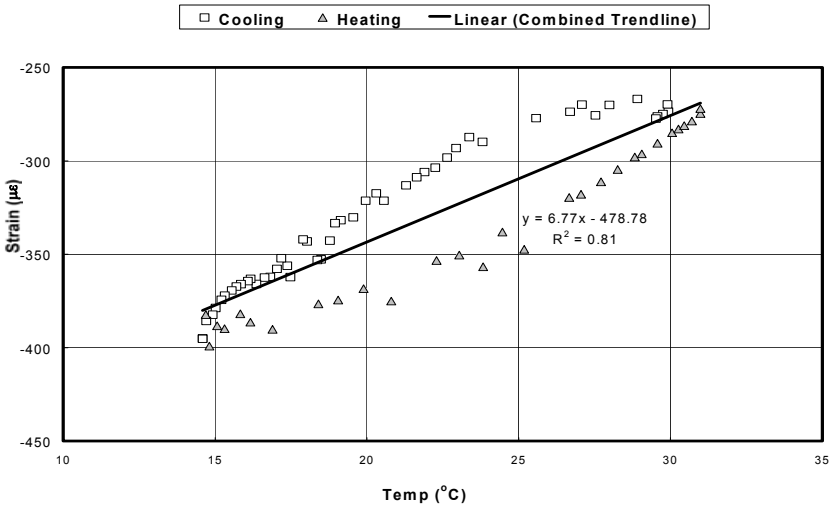

Figure 6: Strain versus temperature for 24 hour period for top VW sensor

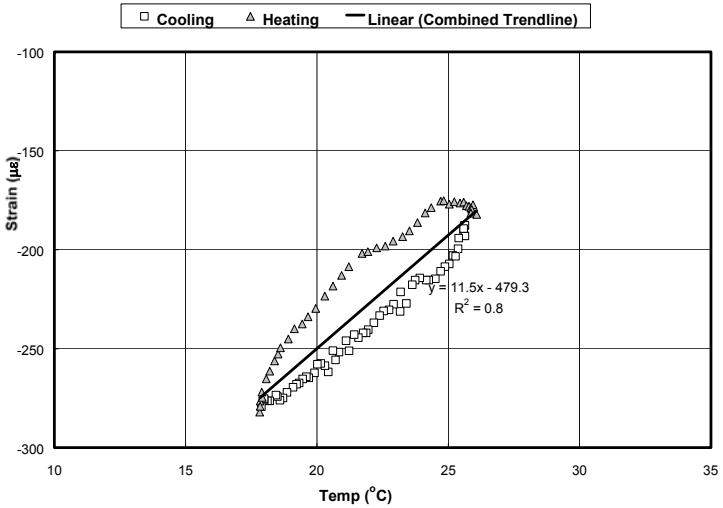

Figure 7: Strain versus temperature for 24 hour period for bottom VW sensor

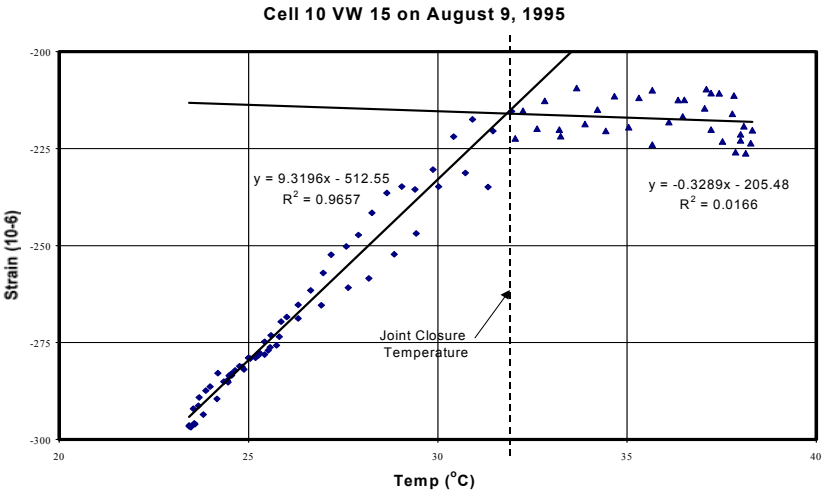

Figure 8: Typical daily strain versus temperature for longitudinal vibrating wire strain sensor (Summer)

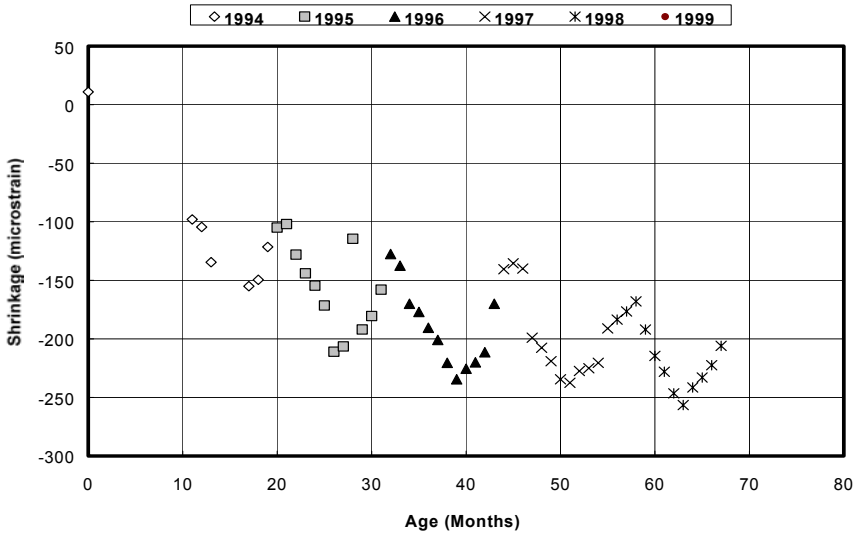

Figure 9: Variability of the drying shrinkage on a monthly basis as the concrete life increases

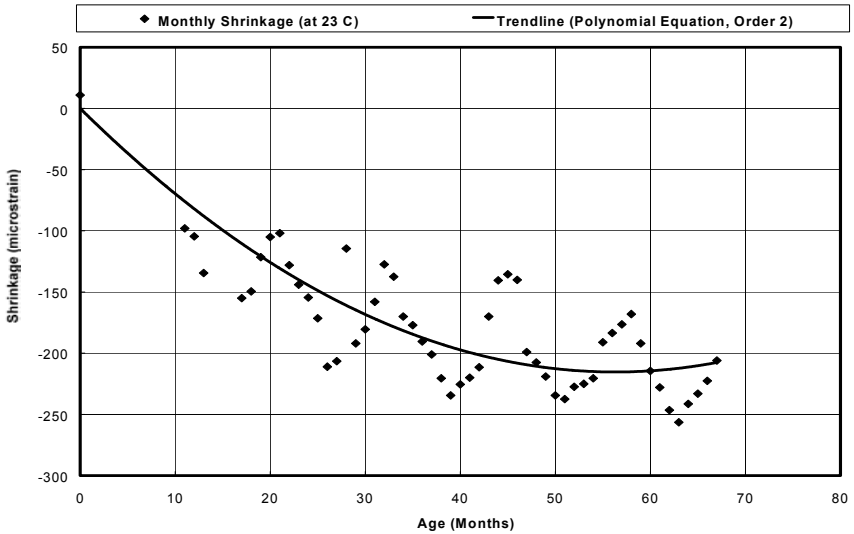

Figure 10: Polynomial best fit line for the variability of drying shrinkage on a monthly basis as concrete life increases

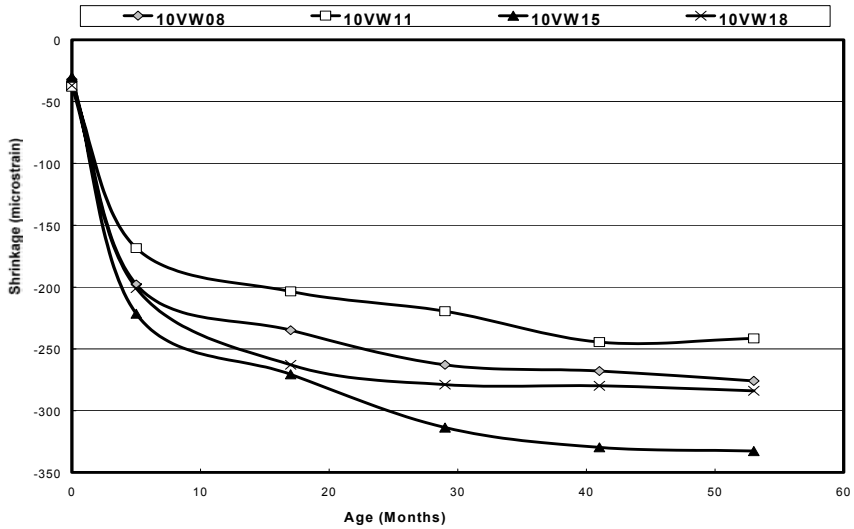

Figure 11: Variability of the drying shrinkage on a monthly basis as the concrete life increases

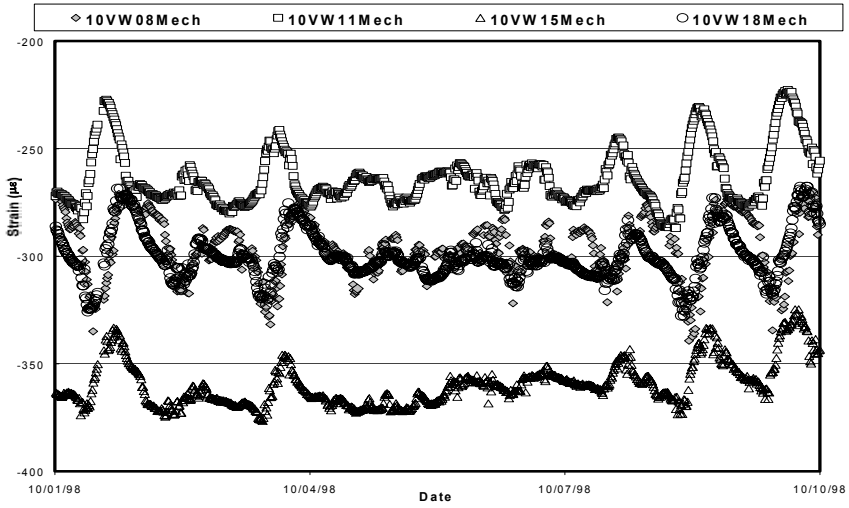

Figure 12: Variability of mechanical strain for one month period

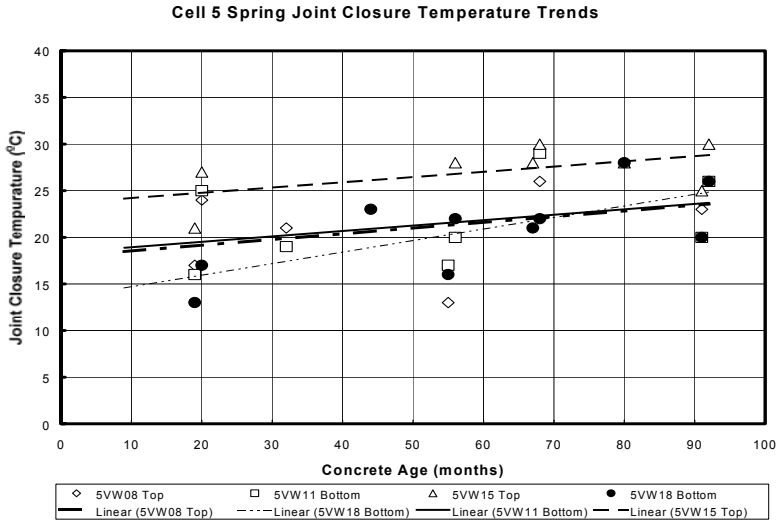

Figure 13: Variation of the joint closure temperature (Spring)

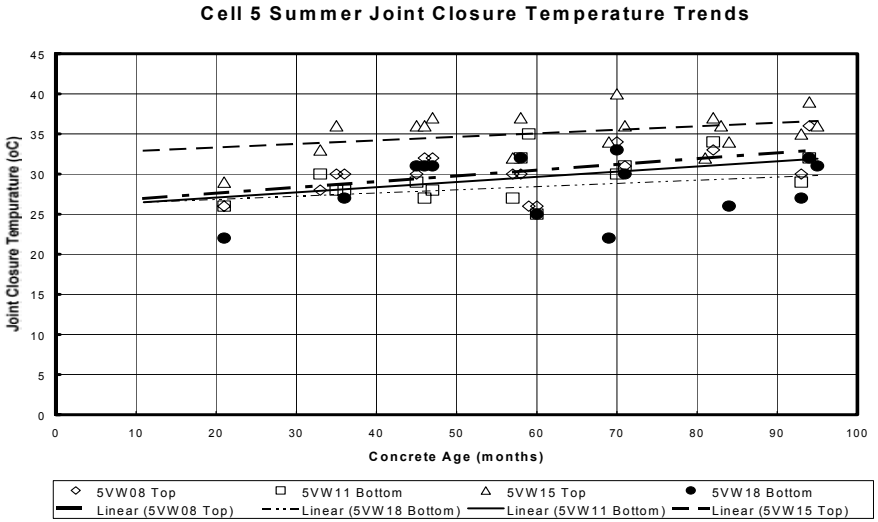

Figure 14: Variation of the joint closure temperature (Summer)